Materials Today Bio 26 (2024) 101102

Contents lists available at ScienceDirect

Materials Today Bio

journal homepage: www.journals.elsevier.com/materials-today-bio

Providing biomimetic microenvironment for pulp regeneration via hydrogel-mediated sustained delivery of tissue-specific developmental signals

Zhuo Xie [a], Peimeng Zhan [a], Xinfang Zhang [a], Shuheng Huang [a], Xuetao Shi [b,***], Zhengmei Lin [a,**], Xianling Gao [a,*]

[a] Hospital of Stomatology, Guanghua School of Stomatology, Sun Yat-sen University, Guangdong Provincial Key Laboratory of Stomatology, Guangzhou, Guangdong, PR China

[b] School of Biomedical Science and Engineering, National Engineering Research Centre for Tissue Restoration and Reconstruction, South China University of Technology, Guangzhou, Guangdong, PR China

ARTICLE INFO

Keywords:
Dentin matrix
Biomimetic hydrogels
Pulp regeneration
Dental pulp stem cells
Tissue engineering

ABSTRACT

Regenerative endodontic therapy is a promising approach to restore the vitality of necrotic teeth, however, pulp regeneration in mature permanent teeth remains a substantial challenge due to insufficient developmental signals. The dentin is embryologically and histologically similar to the pulp, which contains a cocktail of pulp-specific structural proteins and growth factors, thus we proposed an optimizing strategy to obtain dentin matrix extracted proteins (DMEP) and engineered a DMEP functionalized double network hydrogel, whose physicochemical property was tunable by adjusting polymer concentrations to synchronize with regenerated tissues. *In vitro* models showed that the biomimetic hydrogel with sustained release of DMEP provided a beneficial microenvironment for the encapsulation, propagation and migration of human dental pulp stem cells (hDPSCs). The odontogenic and angiogenic differentiation of hDPSCs were enhanced as well. To elicit the mechanism hidden in the microenvironment to guide cell fate, RNA sequencing was performed and 109 differential expression of genes were identified, the majority of which enriched in cell metabolism, cell differentiation and intercellular communications. The involvement of ERK, p38 and JNK MAPK signaling pathways in the process was confirmed. Of note, *in vivo* models showed that the injectable and *in situ* photo-crosslinkable hydrogel was user-friendly for root canal systems and was capable of inducing the regeneration of highly organized and vascularized pulp-like tissues in root segments that subcutaneously implanted into nude mice. Taken together, this study reported a facile and efficient way to fabricate a cell delivery hydrogel with pulp-specific developmental cues, which exhibited promising application and translation potential in future regenerative endodontic fields.

1. Introduction

Dental pulp is a highly vascularized and innervated tissue located within the dentinal wall, providing nutrition and sensation to the entire tooth, also responsible for dentin production, whereas, it is vulnerable to insults rendered from dental caries, accidental trauma and idiopathic factors, which may lead to irreversible pulpitis and pulp necrosis [1]. Pulpless teeth lose their inherent nutritional, sensory and defensive functions, and are prone to fracture, thus the regeneration of pulp tissues deserves an ongoing endeavor [2,3]. Cell-based tissue engineering brought a tremendous revolution to regenerative endodontic fields [3,4]. Autologous human dental pulp stem cells (hDPSCs) transplantation has been reported to induce apexogenesis and regenerate three-dimensional (3D) pulp tissues in young permanent teeth [5]. However, mature permanent teeth with narrow apical foramens could not facilitate sufficient exchange of nutrients and gases to support the survival and function of the transplanted stem cells, also, prepared root canals are incapable of providing adequate odontogenic signals to

* Corresponding author.
** Corresponding author.
*** Corresponding author.
E-mail addresses: shxt@scut.edu.cn (X. Shi), linzhm@mail.sysu.edu.cn (Z. Lin), gaoxling3@mail.sysu.edu.cn (X. Gao).

https://doi.org/10.1016/j.mtbio.2024.101102
Received 8 February 2024; Received in revised form 10 May 2024; Accepted 26 May 2024
Available online 27 May 2024

regulate cell differentiation [6,7]. Thus, it is imperative to bioengineer an odontogenesis-related developmental microenvironment to spur the proliferation and odontogenic differentiation of transplanted hDPSCs and regenerate pulp tissues in mature permanent teeth.

To accomplish this, a multitude of active pharmaceutical agents, possessing potential odontogenic induction capacities, have been explored as biological cues to regulate stem cells fate for pulp regeneration, such as multiple growth factors, bioactive drugs, and synthetic peptides [8,9]. A certain elevated regeneration events could be obtained under these treatments; however, *in vivo* application of recombinant growth factors and small molecules might confront high manufacturing cost, short half-life and potential adverse effects such as intricate crosstalk and ectopic mineralization, most of which have not been clinically approved as well [10,11]. Decellularized extracellular matrix (dECM) is a talented regeneration medicine that presents unique microenvironments for cells to adhere and differentiate [12–14]. The dentin and pulp, both derived from the neuro-mesenchyme of the dental papilla, are embryologically, histologically, and functionally similar tissues, and are covered together as a complex. As such, dentin matrix could be considered as spontaneous dECM rich in a cocktail of pulp tissue-specific structural proteins and natural growth factors to manipulate cell behaviors [15–17]. These molecules fossilized in the mineralized dentin matrix during odontogenesis would function as bioactive components ready to initiate regenerative events after pulp injury [18,19]. The significant role of released dentin matrix-associated bioactive proteins in regenerative endodontics has increasingly been realized by researchers and a number of relational strategies have been proposed such as demineralization treatment and root canal irrigation [18,20,21]. However, it remains challenging to determine the availability and effectiveness of dentin matrix extracted proteins (DMEP) and to deliver them into root canals in a facile way [22,23].

Gels are popular treatment options as their composition can be readily altered to include active agents [3]. Considering the narrow operating space in pulp cavities and the complex and irregular root canals, the injectable and *in situ* photo-crosslinkable hydrogel might be an ideal delivery material compared with preformed scaffolds which are fixed in shapes [24,25]. Gelatin methacrylate (GelMA) and hyaluronic acid methacrylate (HAMA) are modified from collagen I and hyaluronic acid, both of which are major components of the natural ECM [26,27], preserving arginine-glycine-aspartic acid adhesive domains and matrix metalloproteinase (MMP)-sensitive sites that could enhance cell binding and cell-mediated matrix degradation [28]. GelMA and HAMA have been demonstrated to photo-crosslink with each other to form a double network hydrogel and simultaneously retain functional groups, improved mechanical property and degradation rate could be achieved as well [29,30]. Meanwhile, the 3D interior network of the double network hydrogel with appropriate pore size and interconnected porosity is suitable for wrapping cells, cell growth and exchange of nutrients [31].

Based on these premises, we aimed to utilize dentin matrix proteins to develop a biomimetic hydrogel with adequate odontogenic signals for effective pulp regeneration. First, we proposed an optimized scheme advanced in pH value and temperature to efficiently acquire DMEP. Then, a DMEP functionalized GelMA/HAMA hydrogel (DGH) was designed to reproduce the complexity of pulp ECM and mimic the pulp developmental microenvironment via a simplified manufacturing procedure. The biological responses of hDPSCs encapsulated in the biomimetic hydrogel and the mechanism hidden in the odontogenic microenvironment to guide stem cell fates were investigated. Finally, hDPSCs-encapsulated DGH was injected into root segments and subcutaneously implanted into nude mice to evaluate its potential for pulp regeneration.

2. Materials and methods

2.1. Preparation of DMEP

Dentin matrix was obtained from freshly extracted human healthy premolars for orthodontic purposes with informed patient consent in accordance with ethical approval granted by Medical Ethics Committee of Hospital of Stomatology, Sun Yat-Sen University (KQEC-2022-82-01). Soft tissues, enamel and cementum of the teeth were removed, and the remaining dentin was powdered with a grinding mill in liquid nitrogen followed by demineralized in ethylene diamine tetra-acetic acid (EDTA; Aladdin, China) at different concentrations (17 % for 10 min, 10 % for 10min, and 5 % for 5 min). Demineralized dentin matrix (DDM) particles were rinsed with deionized water after each EDTA demineralization and sterilized in a 60 Cobalt gamma irradiator (Gammacell 220 N, Atomic Energy of Canada Ltd., Canada) [16,32]. The irradiation was performed at an average dose rate of 1.55 kGy/h for 16 h and 8 min to achieve the targeted dose of 25 kGy. Subsequently, sterile particles were resuspended in basic solutions (Na_2CO_3/$NaHCO_3$, pH 10) and neutral solutions (phosphate buffer saline, PBS, pH 7.4; Servicebio, China) at 1 g/mL, respectively, then incubated at 4 °C or 37 °C for 72 h. The supernatants containing dissolved proteins in each group were collected and lyophilized to obtain DMEP. Three batches of DMEP were generated and spent for the following experiments.

2.2. Enzyme-linked immunosorbent assay (ELISA)

Customized quantitative multiplex sandwich ELISA kits (Multi-Sciences, China) were employed to determine the concentration of histogenesis-related proteins in DMEP, including transforming growth factor-β1 (TGF-β1), insulin-like growth factor-1 (IGF-1), vascular endothelial growth factor (VEGF), nerve growth factor (NGF) and MMP-9. For each protein, DMEP was reconstituted in calibrator diluent (5 mg/mL) before incubation in microwell plates precoated with monoclonal antibodies to TGF-β1, IGF-1, VEGF, NGF or MMP-9. Serial dilutions of recombinant standards were also incubated to generate a standard curve. Following the 2h-incubation, wells were washed with buffer and incubated with horseradish peroxidase-conjugated polyclonal antibodies to TGF-β1, IGF-1, VEGF, NGF or MMP-9 for 2 h. After washing, the wells were incubated for 30 min with the enzyme substrate solution before the addition of the stop solution. The optical density at a wavelength of 450 nm was read using a microplate reader (BioTek Instruments, USA).

2.3. Synthesis of DGH

GelMA (10 % w/v, DS = 75 %; Engineering For Life, China) and HAMA (2 % w/v, DS = 25 %; Engineering For Life) were dissolved in PBS to harvest the double network hydrogel precursor. Different amounts of DMEP (set as 0 %, 5 %, 10 % and 15 %) were introduced into the hydrogel precursor, named GH, D_5GH, D_{10}GH, and D_{15}GH. Sodium hydroxide (0.5 M) and hydrochloric acid (0.5 M) were used to bring the pH of the mixed solution to between 7.3 and 7.5. To form the hydrogel, photoinitiator LAP (0.25 % w/v; Engineering For Life) was added with subsequent exposure to UV light (405 nm, 25 mW/cm^2) for 20 s.

2.4. Scanning electron microscopy (SEM)

To characterize the internal microstructure of DGH and the granulometric distribution of DMEP, hydrogel samples were lyophilized and cut off after embrittlement in liquid nitrogen, sprayed with gold on the surface and cross-section, and then placed under field emission SEM (FEI QUANTA 200, USA) for observation.

2.5. Rheology analysis

Rheological properties of hydrogels were measured using a stress-controlled rheometer (DHR-2, TA instruments, USA) fitted with a Peltier stage. Hydrogel samples with a diameter of 8 mm and thickness of 1 mm were prepared, by applying UV-initiated polymerization of the monomer mixture in a polytetrafluoroethylene mold. In accordance with the previous research, a TA Discovery Series HR-1 Rheometer 8 mm parallel plate mold was used. Examinations were performed using oscillatory frequency sweeps (0.1–10 Hz, 1 % strain) to record the storage modulus and loss modulus [33]. All the tests were performed at room temperature.

2.6. Mechanical analysis

Mechanical performances of hydrogels were characterized on a dynamic mechanical analyzer (Q800 DMA, TA instruments, USA). Compression tests were applied to the surface of cylindrical hydrogel specimens (diameter: 9 mm; height: 5 mm) at 5 % strain/min after preconditioning for 10 cycles (1–5 % strain) at 0.5 Hz frequency. The linear part of each stress-strain curve was used to calculate the compression modulus. For tensile tests, rectangular hydrogel specimens with dimensions around 20 mm (length) × 4 mm (width) × 0.8 mm (thickness) were used, and a constant crosshead speed of 50 mm/min was applied. Cyclic tensile measurements were performed at various predetermined maximum strains. All the mechanical tests were conducted at room temperature.

2.7. In vivo degradation assay and biocompatibility assay

Hydrogel samples (diameter: 9 mm; height: 5 mm) were subcutaneously implanted into BALB/C nude mice (6–8 wks, male) to evaluate degradability in accordance with ethical approval granted by the Animal Care and Use Committee of Sun Yat-Sen University (SYSU-IACUC-2022-000036). Mice were divided into 3 groups: the PBS group, the GH group, and the DGH group (n = 5 per group). At 2-, 4-, 6-, and 8-week post-operation, hydrogel samples were harvested for assessment of weight alteration. The sample-surrounding tissues, as well as hearts, livers, spleens, lungs, and kidneys of the mice were harvested for H&E stain (Solarbio, China) to evaluate biocompatibility. All stained sections were observed under a slide scanner (Aperio AT2; Leica Biosystems, Germany).

2.8. Cell isolation and identification

As described in our previous literature, hDPSCs were isolated from 18- to 25-year-old healthy volunteers (n = 6) with ethical approval (KQEC-2022-82-01) and informed consent [34]. Cells were cultured in α-MEM medium (GIBCO, Australia) supplemented with 20 % fetal bovine serum (FBS; GIBCO) and 1 % penicillin-streptomycin (P/S; Sigma, USA) at 37 °C in a 5 % CO_2 high-humidity environment. The medium was replaced every 3 days and hDPSCs at passages 3–5 were used for following experiments. To evaluate the osteogenic differentiation potential of stem cells, hDPSCs underwent induction for 21 days with osteogenic medium (Cyagen, China) and stained with alizarin red S (ARS) solution (Cyagen). To evaluate the adipogenic differentiation, hDPSCs underwent culture for 28 days in adipogenic medium (Cyagen) and stained with oil red O solution (Cyagen). Flow cytometry analysis was performed to investigate hDPSCs for surface markers. Cells were incubated with conjugated human antibodies including CD29-FITC, CD44-APC, CD90-PE, CD34-FITC and CD45-PE (BD, USA), and assessed flow cytometrically (BD).

2.9. Cytoskeleton staining, live/dead assay, and Cell Counting Kit-8 (CCK-8) assay

For 3D culture, hDPSCs (10×10^4 per well) were resuspended with hydrogel precursor solutions uniformly, then hDPSCs-encapsulated hydrogels were immediately and carefully injected into 12-well plates, followed by irradiated with UV light for 20 s and soaked with culture medium. To detect cell spreading, hDPSCs-encapsulated hydrogels cultured for 1, 3 and 7 days were fixed with 4 % paraformaldehyde (Biosharp, China), then stained with Alexa Fluor 488 phalloidin (Sigma) and DAPI (Sigma) to remark f-actin filaments and nuclei. Stained samples were observed by confocal laser scanning microscope (CLSM; Olympus FV3000, Japan). To detect cell viability, hDPSCs-encapsulated hydrogels cultured for 7 days were stained by a Calcein-AM/PI Double Stain Kit (Yeasen, China) and stained samples were observed by CLSM. To monitor cell proliferation, hDPSCs-encapsulated hydrogels cultured for 1, 3, 5, 7, 10 and 14 days were stained with CCK-8 (Dojindo, Japan) and absorbance at 450 nm was measured as a quantitative indicator of cell numbers.

2.10. Cell migration

Cell migration was tested with 8 μm pore size Transwell@ cell culture set (Corning, USA). Following a 12 h-serum starvation, hDPSCs suspension (5×10^4 per well) was plated in the insert in 200 μL α-MEM medium. In the lower chamber, hydrogels were immersed in 750 μL α-MEM medium. Following a 24 h- and 48 h-incubation, cells migrated to the lower filter were fixed with 4 % paraformaldehyde, stained with 0.1 % crystal violet, and counted under an inverted fluorescence microscope (Olympus IX83, Japan).

2.11. Alkaline phosphatase (ALP) and ARS staining assays

To evaluate the early odontogenic differentiation, hDPSCs-encapsulated hydrogels at day 7 were fixed with 4 % paraformaldehyde and stained with the BCIP/NBT ALP Colorimetric Kit (Beyotime, China) according to the manufacturer's instructions. Stained samples were decolorized with 2 M KOH and DMSO (Absin, China) and absorbance at 620 nm was measured as a quantitative indicator of blue formazan [35]. To assess matrix mineralization in the late stage, hDPSCs-encapsulated hydrogels at day 21 were stained with ARS solution. Stained samples were decolorized with 10 % cetylpyridinium chloride (Adamas, China) and absorbance at 562 nm was measured as a quantitative indicator of calcium concentration.

2.12. Quantitative real-time polymerase chain reaction (qRT-PCR) assay

To investigate the expressions of odontogenesis- and angiogenesis-related genes in hDPSCs, hDPSCs-encapsulated hydrogels at day 14 were frozen in liquid nitrogen and ground into powder at subzero temperatures. The total RNA of cells was extracted with NucleoZOL reagent (Gene Company Limited, China) and reverse-transcribed into cDNA using PrimeScript RT Master Mix (TaKaRa, Japan). The mRNA expression of *COL-1*, *DSPP*, *DMP-1*, *VEGFA* and *OCN* was measured by qRT-PCR with SYBR Green assays (Yeasen). Glyceraldehyde 3-phosphate dehydrogenase (*GAPDH*) was used as an internal control, and the relative level of gene expression was calculated based on the $2^{-\Delta\Delta Ct}$ method. Primer sequences used were listed in Table 1.

2.13. Western blotting

To investigate the expressions of odontogenesis- and angiogenesis-related proteins, hDPSCs-encapsulated hydrogels at day 14 were frozen in liquid nitrogen and ground into powder at subzero temperatures. The total proteins of cells were extracted by RIPA Lysis Buffer (CWBio, China) with 1 % PMSF (CWBio). Proteins were separated on a

Table 1
Primer sequences for qRT-PCR.

Gene	Forward primer (5′-3′)	Reverse primer (5′-3′)
COL-1	GAGGGCCAAGACGAAGACATC	CAGATCACGTCATCGCACAAC
DSPP	GGGATGTTGGCGATGCA	CCAGCTACTTGAGGTCCATCTTC
DMP-1	AGGAAGTCTCGCATCTCAGAG	TGGAGTTGCTGTTTTCTGTAGAG
VEGFA	AGGGCAGAATCATCACGAAGT	AGGGTCTCGATTGGATGGCA
OCN	AGCAAAGGTGCAGCCTTTGT	GCGCCTGGGTCTCTTCACT
GAPDH	GGGAAACTGTGGCGTGAT	GAGTGGGTGTCGCTGTTGA

4–20 % SDS-PAGE gel (Smart-Lifesciences, China), transferred to PVDF membranes (Millipore, USA), and detected with anti-COL-1 (R26615, 1:1000, ZENBIO, China), anti-DSPP (sc-73632, 1:200, Santa Cruz Biotechnology, USA), anti-DMP-1 (AP18965a, 1:1000, Abcepta, China), anti-VEGFA (R26073, 1:1000, ZENBIO), anti-OCN (614487, 1:1000, ZENBIO) and anti-β-actin (bsm-33036 M, 1:5000, Bioss Antibodies, China). After incubating with the secondary antibody (Asbio Technology, China) for 1 h, the signals were observed via the western blotting detection system (Bio-Rad, USA). Protein bands were quantified using ImageJ (Version 1.8.0; NIH Image software, USA).

2.14. Immunofluorescence staining

To visualize the expression of above proteins, hDPSCs-encapsulated hydrogels at day 14 were fixed with 4 % paraformaldehyde, permeabilized with 0.1 % Triton X-100 (Sigma) and blocked with 3 % bovine serum albumin (BSA; BioFroxx, China). The hydrogels were then incubated with primary antibodies including COL-1 (AF7001, 1:100, Affinity Biosciences, USA), DSPP (sc-73632, 1:50, Santa Cruz Biotechnology), DMP-1 (sc-73633, 1:50, Santa Cruz Biotechnology), VEGFA (sc-7269, 1:50, Santa Cruz Biotechnology) and OCN (23418-1-AP, 1:50, Proteintech Group, USA) overnight at 4 °C, followed by incubated with secondary antibodies (Alexa Fluor 594, EMARBIO Science & Tech, China) for 1 h. The cell f-actin filaments and nuclei were stained with Alexa Fluor 488 phalloidin and DAPI. Stained samples were observed by Olympus FV3000.

2.15. Transcriptome analysis by RNA sequencing (RNA-seq)

To explore the underlying mechanism of cell differentiation induced by DGH, total RNA was isolated from hDPSCs encapsulated in GH and D_{10}GH for 14 days with NucleoZOL reagent. RNA-seq libraries were prepared with the NEBNext® UltraTM RNA Library Prep Kit (NEB, USA), followed by sequencing with Illumina Sequencing (HiSeq, Fasteris SA, Switzerland) at Berry Genomics (Beijing, China). Feature counts were used to calculate read counts, and DESeq2 was used to analyze the differential expression of genes (DEGs). Genes with a corrected *p*-value <0.05 and an absolute log2 (fold-change) > 2 were considered differentially expressed. GO enrichment analysis of the top 100 DEGs was performed with the Database for Annotation, Visualization and Integrated Discovery (DAVID).

2.16. ERK, p38 and JNK MAPK inhibition assay

To determine the role of MAPK signaling pathways in DGH-mediated cell differentiation, hDPSCs-encapsulated hydrogels were treated with ERK inhibitor U0126 (10 μM; Invivogen, USA), p38 inhibitor SB203580 (10 μM; Invivogen) or JNK inhibitor SP600125 (10 μM; Invivogen) for 60 min, then relative protein levels were detected with anti-phospho-p38 (#4511, 1:1000, Cell Signaling Technology, USA), anti-p38 (#8690, 1:1000, Cell Signaling Technology), anti-phospho-ERK1/2 (301245, 1:1000, ZENBIO), anti-ERK1/2 (#4695, 1:1000, Cell Signaling Technology), anti-phospho-JNK (381100, 1:1000, ZENBIO) and anti-JNK (#9252, 1:2000, Cell Signaling Technology). ALP assay, ARS assay and western blotting were performed as described above.

2.17. Subcutaneous implantation of root segments

Human root segments were obtained from freshly extracted single rooted premolars and prepared for 5–6 mm in length using a diamond bur, reserving the narrow apical foramen of each segment to mimic the clinical situation. All segments were soaked in 17 % EDTA for 10 min and in 19 % citric acid for 1 min to remove the smear layer, then sterilized using Co-60 irradiation. Subsequently, pure hDPSCs and hDPSCs resuspended with hydrogel precursors (about 2×10^4/20 μL per segment) were injected into root segments and irradiated with UV light to crosslink. Root segments were divided into 3 groups: the pure cells group, the GH group, and the DGH group ($n = 5$ per group). All root segments were soaked in culture medium for 3 days. Then, the coronal end of each segment was sealed with iRoot BP Plus (Innovative BioCeramix Inc., Canada) and implanted into subcutaneous pockets of BALB/C nude mice (6–8wks, male). All experiments were approved by the Animal Care and Use Committee of Sun Yat-Sen University (SYSU-IACUC-2022-001299). The mice were euthanized via the Ethics Committees approved methods at 12 weeks for analysis of the implants.

2.18. Histological staining

Harvested specimens were immediately fixed in 4 % formaldehyde for 24 h, demineralized in 10 % EDTA for 12 weeks, dehydrated and embedded in paraffin. Sections (5 μm thick) were coronally cut longitudinally and stained with H&E (Solarbio) as well as Masson's trichrome (Solarbio). Primary antibodies against DSPP (sc-73632, 1:50, Santa Cruz Biotechnology) and CD31 (AF6191, 1:50, Affinity Biosciences) were used for immunofluorescence staining to detect regenerated pulp tissues and blood vessels *in vivo*. To verify that nascent tissues were formed from implanted hDPSCs, tissue sections were co-stained for COXIV (FineTest, China). Alexa Fluor 594 and 488 were used as secondary antibodies. Stained samples were observed by Olympus FV3000. Three regions of a root section were randomly selected to quantify positive expression. The number of anti-DSPP positive cells/total counted cells and the rate of neovascularization were calculated by ImageJ.

2.19. Statistical analysis

All data are presented as the means ± SEMs of at least 3 independent experiments. Comparisons between groups were performed using one-way ANOVA with Tukey's post hoc test, and $p < 0.05$ was considered statistically significant. All statistical analyses were performed with GraphPad Prism 9.0 (GraphPad Software, USA).

3. Results

3.1. Alkaline- and temperature-activated release of DMEP

Dentin matrix was obtained from freshly extracted human healthy premolars, powdered into particles, and demineralized with EDTA (Fig. 1A). SEM showed that dentinal tubules were exposed after demineralization treatment, which allowed endogenous bioactive molecules to release into the surroundings (Fig. 1B). The average size of DDM particles was 526.2 ± 210.3 μm (Fig. 1B and C). Then, DMEP was extracted from dentin matrix particles, the diameter of which was approximately 1.455 ± 0.433 μm (Fig. 1D and E). The pH value-/temperature-mediated release efficiency of multiple proteins from dentin matrix was evaluated by ELISA. In four groups, DMEP at pH 7.4/4 °C possessed the minimum release efficiency, while the release amounts were respectively increased under alkaline treatment and elevated temperature treatment (Fig. 1F). TGF-β1 and NGF in DMEP at pH 10/37 °C were 5.33- and 3.68-fold higher than those at pH 7.4/4 °C (Fig. 1F). Interestingly, the release kinetics of TGF-β1, NGF, and MMP-9 presented a steady growth during 72 h, while IGF-1 and VEGF occurred a burst release after 24h-incubation (Fig. 1F). Considering the maximum

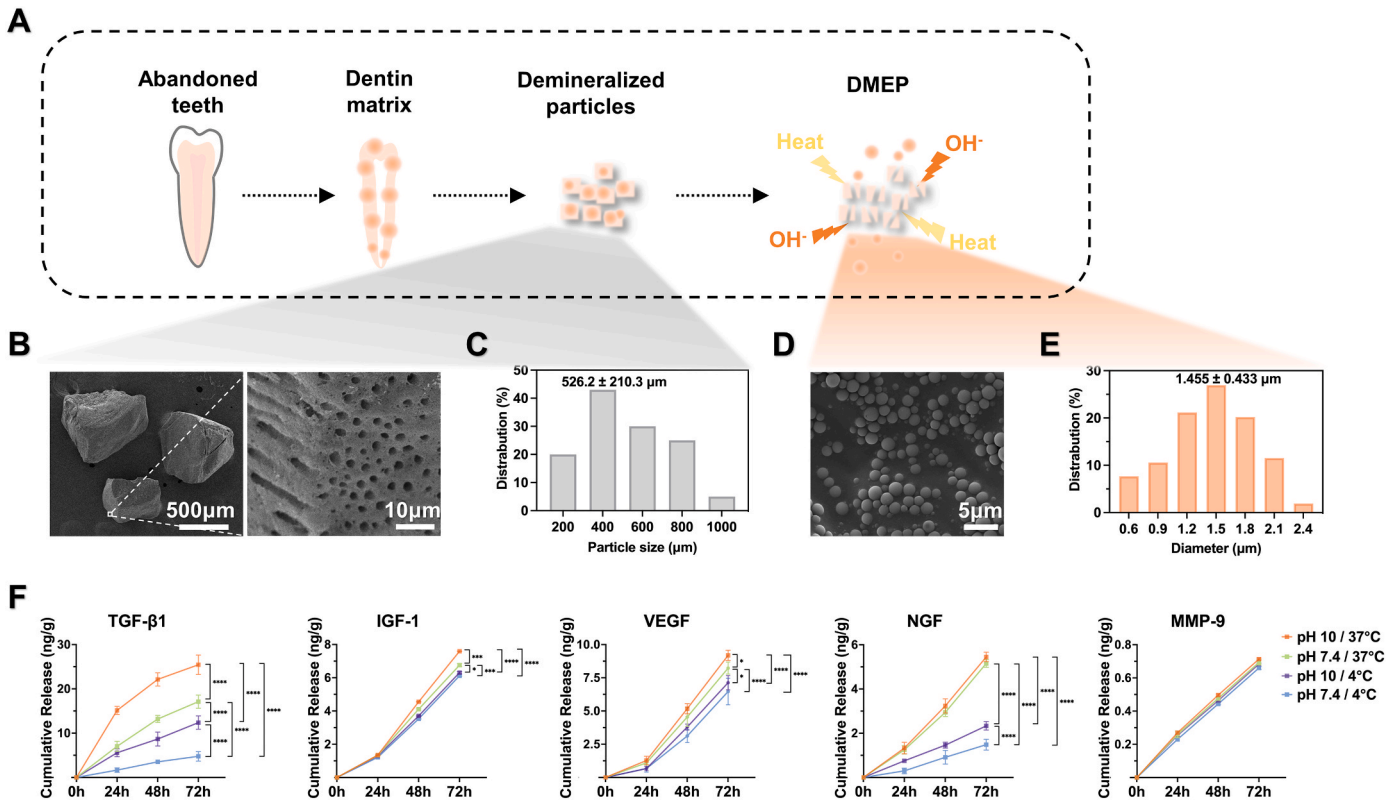

Fig. 1. Preparation of dentin matrix extracted proteins (DMEP). (A) Synthetic route of demineralized dentin matrix (DDM) particles and DMEP. (B) SEM image of DDM particles. Insets in the right region are magnified images of the rectangles. Scale bar of the left panels: 500 μm; scale bar of the right panels: 10 μm. (C) Particle size analysis of DDM particles from SEM images. (D) SEM image of DMEP. Scale bar: 5 μm. (E) Diameter analysis of DMEP from SEM images. (F) Release pattern of TGF-β1, IGF-1, VEGF, NGF and MMP-9 from dentin matrix under different pH values and temperatures. ****$p < 0.0001$, ***$p < 0.001$, *$p < 0.05$.

enrichment of growth factors, DMEP incubated at pH 10/37 °C was our focus in subsequent experiments.

3.2. Physicochemical properties of DGH

DMEP was incorporated into the GelMA/HAMA double network precursor to construct the DGH hydrogel (Fig. 2A). DGH was injectable and could be *in situ* photo-crosslinked after exposing to UV radiation for 20 s (Fig. 2B and C). The lyophilized hydrogel presented a porous internal structure with connected pores (approximately 80 μm) (Fig. 2D). According to rheological characterization, all four hydrogel groups exhibited an elastic, solid-like behavior (storage modulus > loss modulus) after ultraviolet radiation in a short time and the storage modulus increased with the DMEP content (Fig. 2E). However, when the DMEP content reached 15 %, the storage modulus of the hydrogel decreased, probably due to high concentration and uneven distribution of DMEP within the hydrogel and resultant light obstruction in the UV crosslinking process. Mechanical properties must also be considered when developing a tissue engineering hydrogel scaffold. DGH exhibited a ~1.5-fold increase in compressive modulus compared to GH, while those of D_5GH, D_{10}GH and D_{15}GH samples were of no significant difference (Fig. 2F). Similarly, the Young's modulus of DMEP-loaded hydrogels was found with an augmentation of 30 % than GH, indicating the positive effect of DMEP on hydrogel strength (Fig. 2G).

Additionally, *in vivo* degradation assay was performed to detect the degradability of hydrogels. A continuous and relatively stable degradation was observed, while the degradation rate of DGH was tardier than GH, whose remained mass at 8-week post-implantation was 17.68 % ± 4.48 % and 11.25 % ± 6.35 %, respectively (Fig. 2H). At 4-week after implantation, a moderate inflammatory response was observed in the tissue around GH, and the representative inflammatory cells were enclosed by a black frame (Fig. 2I). Interestingly, the host response against DGH revealed weaker. After 8 weeks, only a few inflammatory cells were left in the hydrogel-implanted sites, indicating no obvious difference with the PBS group. H&E staining of the hearts, livers, spleens, lungs, and kidneys did not reveal any noticeable systemic toxicity, suggesting no significant damage to the major organs after implantation of hydrogels (Fig. 2J).

3.3. Biological assessment of hDPSCs encapsulated in DGH

Primary hDPSCs (Fig. 3A) were isolated and cells at passage 3 (Fig. 3B) were examined. As shown in Fig. 3C and D, hDPSCs could differentiate into osteoblasts and adipocytes, suggesting their multilineage differentiation potential. Flow cytometry analysis showed that hDPSCs presented low CD34 and CD45 (hematopoietic cell marker) amounts (0.27 % and 1.25 %), but elevated amounts of the mesenchymal stem cell markers CD29 (99.05 %), CD44 (99.98 %) and CD90 (98.72 %) (Fig. 3E).

To detect the biological effect of DGH as a cell delivery material, the spreading, viability and proliferation behaviors of hDPSCs encapsulated in hydrogels were assessed. First, cytoskeleton staining was performed to observe cell spreading morphology. In the initial 3 days, hDPSCs displayed a spherical morphology without stress fibers especially those encapsulated in relatively high crosslinking networks (D_{15}GH) (Fig. 3F), properly due to the spatially hindering by the surrounding matrix in the 3D microenvironment. Subsequently, hDPSCs gradually extended into a well-spread morphology, in which obvious filopodia and elongated actin fibers could be observed. The extension speed and extent of hDPSCs encapsulated in D_{15}GH were slightly lower than other groups. Second, the viability of hDPSCs encapsulated in hydrogels for 7 days was ascertained by the live/dead assay. All the fluorescence images were

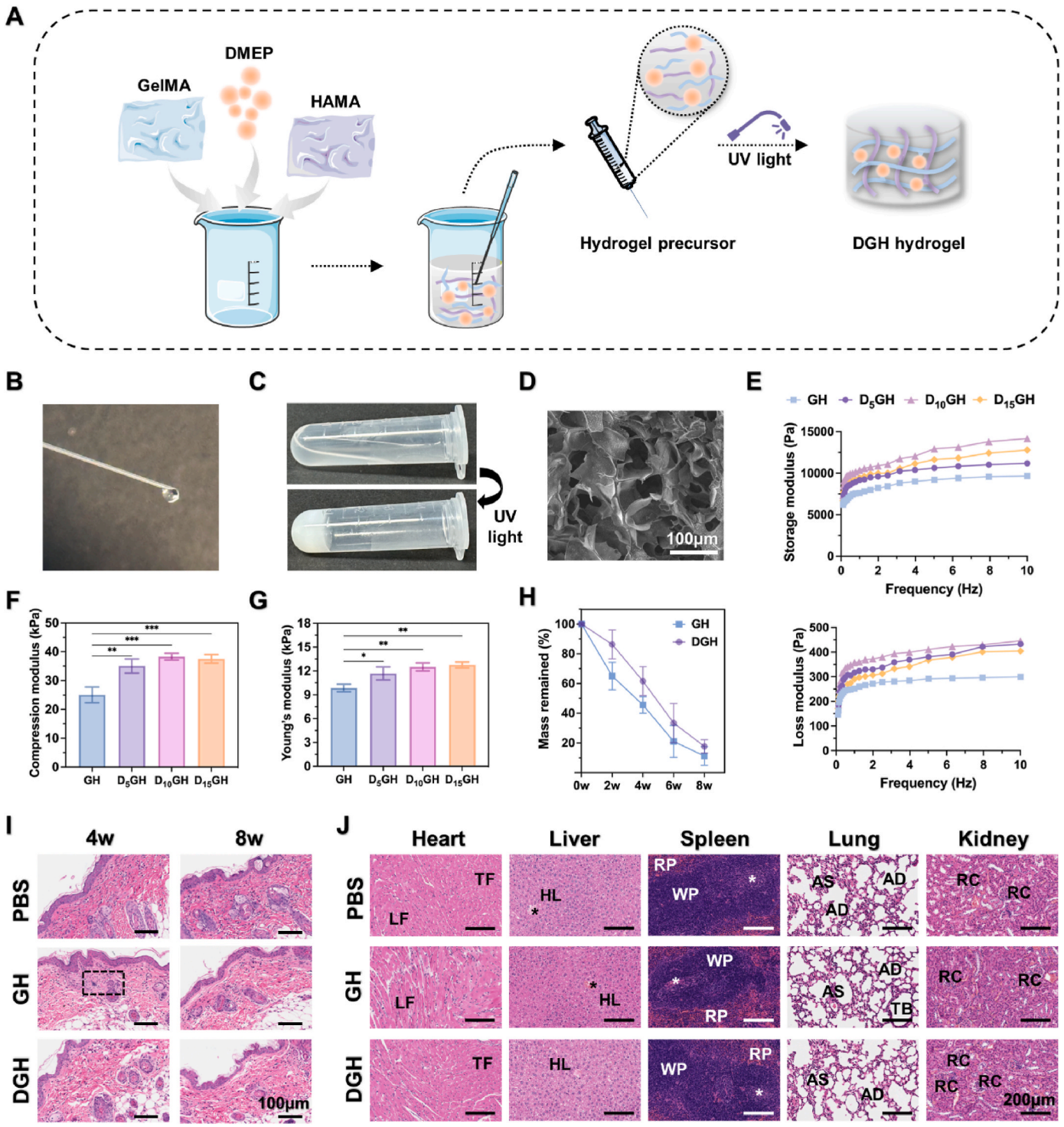

Fig. 2. Synthesis and characterization of DGH. (A) Synthetic route of DGH. (B) The injectable statement of DGH can be administered using a syringe needle. (C) DGH transformed from solution into a gel after UV crosslinking. (D) SEM image of internal microstructure of DGH. Scale bar: 100 μm. (E) Rheological performance of GH, D_5GH, D_{10}GH and D_{15}GH. (F) Compression modulus of GH, D_5GH, D_{10}GH and D_{15}GH. (G) Young's modulus of GH, D_5GH, D_{10}GH and D_{15}GH. (H) *In vivo* degradation rate of GH and DGH after subcutaneous implantation into BALB/C nude mice. (I) H&E staining of tissues around GH and DGH at 4 and 8 weeks after implantation. PBS was set as the blank control. Representative inflammatory cells are indicated by black asterisks. Scale bar: 100 μm. (J) H&E staining of hearts, livers, spleens, lungs, and kidneys of the mice after implantation of GH and DGH. LF represents longitudinal myocardial fibers, TF represents transverse myocardial fibers, HL represents hepatic lobules, black stars indicate central veins, RP represents red pulp, WP represents white pulp, white stars indicate central arteries, AD represents alveolar ducts, AS represents alveolar sacs, TB represents terminal bronchioles, and RC represents renal corpuscles. Scale bar: 200 μm. ***$p < 0.001$, **$p < 0.01$, *$p < 0.05$. (For interpretation of the references to colour in this figure legend, the reader is referred to the Web version of this article.)

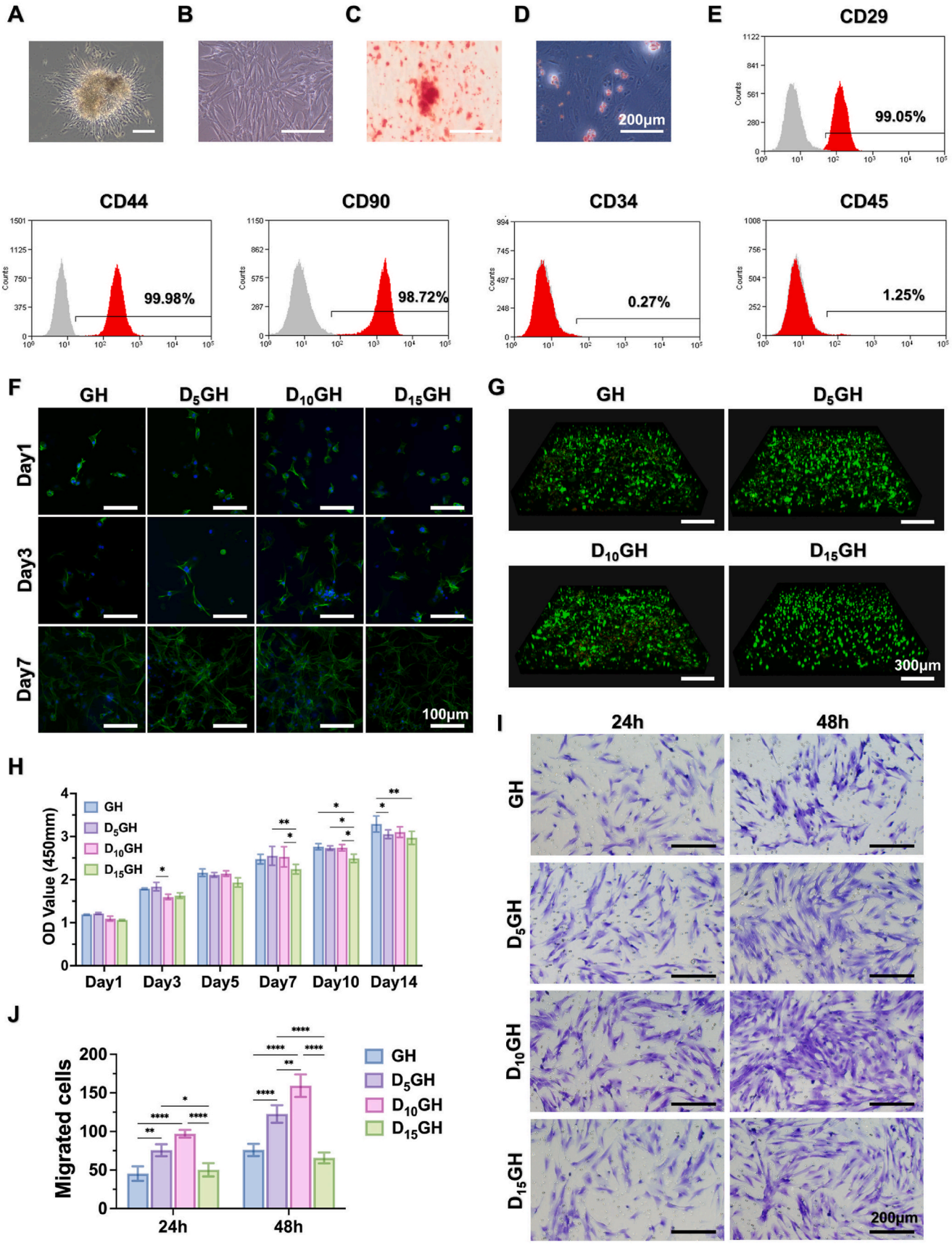

(caption on next page)

Fig. 3. Biological assessment of human dental pulp stem cells (hDPSCs) encapsulated in hydrogels. (A) Morphology of primary hDPSCs at day 5. (B) Morphology of hDPSCs at passage 3. (C) Alizarin red S (ARS) staining of hDPSCs after osteogenic induction for 21 days. (D) Oil red O staining of hDPSCs after adipogenic induction for 28 days. Scale bar: 200 μm. (E) Flow cytometry analysis of surface markers (CD29, CD44, CD90, CD34 and CD45) of hDPSCs. (F) Fluorescence microscopy images of spread morphology of hDPSCs encapsulated in hydrogels at day 1, 3, and 7. F-actin was stained green and nuclei were stained blue. Scale bar: 100 μm. (G) Live/dead assay of hDPSCs encapsulated in hydrogels at day 1, 3, and 7. Live cells were stained green and dead cells were stained red. Scale bar: 300 μm. (H) Cell Counting Kit-8 (CCK-8) assay of hDPSCs encapsulated in hydrogels from day 1 to day 14. (I) Transwell assay of hDPSCs exposed to hydrogels Scale bar: 200 μm. (J) Quantitative analysis of migrated cell numbers. $^{****}p < 0.0001$, $^{**}p < 0.01$, $^{*}p < 0.05$. (For interpretation of the references to colour in this figure legend, the reader is referred to the Web version of this article.)

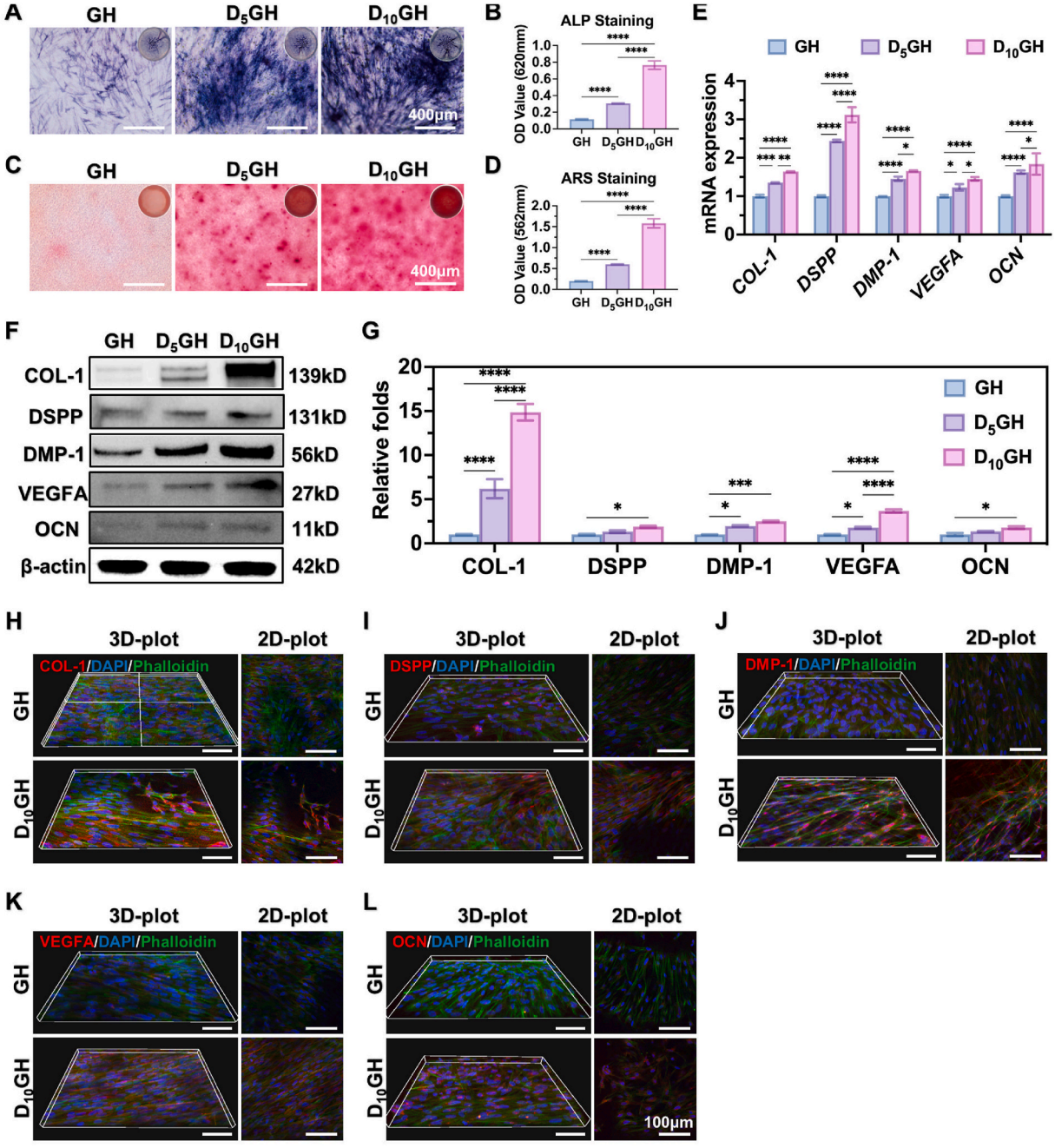

Fig. 4. Odontogenic and angiogenic differentiation of hDPSCs encapsulated in hydrogels. (A) Alkaline phosphatase (ALP) staining of hDPSCs-encapsulated hydrogels at day 7. Scale bar: 400 μm. (B) Quantitative analysis of ALP activity. (C) ARS staining of hDPSCs-encapsulated hydrogels at day 14. Scale bar: 400 μm. (D) Quantitative analysis of mineralized nodules. (E) The mRNA expression of *COL-1*, *DSPP*, *DMP-1*, *VEGFA* and *OCN* in hDPSCs encapsulated in hydrogels. (F) The expression of COL-1, DSPP, DMP-1, VEGFA and OCN proteins in hDPSCs encapsulated in hydrogels. (G) Quantitative analysis of COL-1, DSPP, DMP-1, VEGFA and OCN proteins. (H–L) Immunofluorescence staining of COL-1, DSPP, DMP-1, VEGFA and OCN in hDPSCs encapsulated in hydrogels. Target proteins were stained red, f-actin was stained green, and nuclei were stained blue. Scale bar: 100 μm. $^{****}p < 0.0001$, $^{***}p < 0.001$, $^{**}p < 0.01$, $^{*}p < 0.05$. (For interpretation of the references to colour in this figure legend, the reader is referred to the Web version of this article.)

dominated by intense green fluorescence (live cells) and only very little red fluorescence (dead cells) was observed (Fig. 3G). Next, CCK-8 assay revealed that hDPSCs survived and proliferated well in hydrogels within a 14-day culture, whereas the cell density in the D_{15}GH group at day 7, 10 and 14 was obviously lower than other groups ($p < 0.05$) (Fig. 3H). Eventually, the migration of hDPSCs exposed to hydrogels was detected by the transwell assay (Fig. 3I). D_5GH and D_{10}GH exhibited powerful abilities to recruit hDPSCs, in the presence of which, 1.7- and 2.1-fold increases in migrated cells were observed, respectively, while the motility of hDPSCs exposed to D_{15}GH was similar to the GH group ($p > 0.05$) (Fig. 3J).

Taken together, our results indicated that the double network hydrogel was tunable and capable of tuning cell-matrix interactions and guiding cell shapes. Due to biological and mechanical alterations, either alone or in concert, the adequate addition of DMEP into the crosslinked hydrogel (D_5GH and D_{10}GH) could provide a better 3D microenvironment for cell survival, metabolism and recruitment, while over-utilization of DMEP such as D_{15}GH was profitless. Thus, we selected D_5GH and D_{10}GH as candidates for subsequent cell differentiation investigation.

3.4. Promotion of odontogenic and angiogenic differentiation of hDPSCs encapsulated in DGH

To investigate whether the microenvironment provided by DGH could enhance odontogenic and angiogenic differentiation of seed cells, ALP assay, ARS assay, qRT-PCR, western blotting and immunofluorescence staining were performed. ALP production at day 7 was profoundly promoted in the D_5GH and D_{10}GH group, by 2.7- and 6.6-fold, respectively (Fig. 4A and B). ALP is a critical marker in the early stage of odontogenic differentiation, and its high activity leads to the acceleration of the mineralization process. ARS assay at day 21 revealed that the formation of mineralized nodules was elevated by 3.0- and 8.0-fold in the D_5GH and D_{10}GH group, which was consistent with ALP activity (Fig. 4C and D). Then, the expression of odontogenesis- and angiogenesis-related genes of hDPSCs encapsulated in hydrogels was detected by qRT-PCR. Compared with GH, D_5GH upregulated the expression of *COL-1*, *DSPP*, *DMP-1*, *VEGFA* and *OCN* by ~1.2- to 2.4-fold, while D_{10}GH promoted the highest expression of aforementioned genes by ~1.5- to 3.1-fold (Fig. 4E). Western blotting results showed that D_5GH stimulated an increase in the expression of COL-1, DMP-1 and VEGFA, but did not obviously alter the DSPP and OCN expression ($p > 0.05$) (Fig. 4F and G). Notably, the expression of COL-1, DSPP, DMP-1, VEGFA and OCN in D_{10}GH was prominent among all the groups (Fig. 4F and G). To visualize the expression of relevant proteins, fluorescently labeled COL-1, DSPP, DMP-1, VEGFA and OCN proteins in hDPSCs-encapsulated hydrogels were identified. The GH group showed weak red fluorescent signals, while red fluorescence in D_{10}GH was relatively stronger, indicating higher odontogenesis- and angiogenesis-related proteins production (Fig. 4H-L). Of note, labeled COL-1 protein was also detected in the ECM area of the D_{10}GH group, which might attribute to the combination effects of enhanced ECM secretion and original COL-1 binding sites preserved in hydrogels (Fig. 4H).

3.5. Involvement of MAPK signaling pathways in DGH-mediated cell differentiation

RNA-seq was performed to elucidate the mechanism of guiding cell differentiation hidden in the biomimetic microenvironment of DGH. Compared to the GH group, hDPSCs encapsulated in DGH resulted in 109 DEGs, including 63 upregulated and 46 downregulated (Fig. 5A and B). In GO analysis, these DEGs were mostly involved in nerve development, epithelial cell differentiation, protein maturation, regulated secretory pathways, response to stimulus, cell communication, plasma membrane, NGF receptor activity and so on (Fig. 5C). KEGG pathway analysis revealed that MAPK signaling pathways might be activated by DGH during cell differentiation process (Fig. 5D). Coincidentally, ERK, p38 and JNK MAPK were demonstrated as positive targets for the odontogenic differentiation of hDPSCs in our previous studies [36,37].

To verify whether MAPK signals were involved in DGH-mediated cell differentiation, the expressions of phosphorylated ERK, p38 and JNK MAPK proteins in hDPSCs encapsulated in GH and DGH were detected (Fig. 6A). The ratios of *p*-ERK/ERK, p-p38/p38 and *p*-JNK/JNK in the DGH group were found with an augmentation of 36.3 %, 33.1 % and

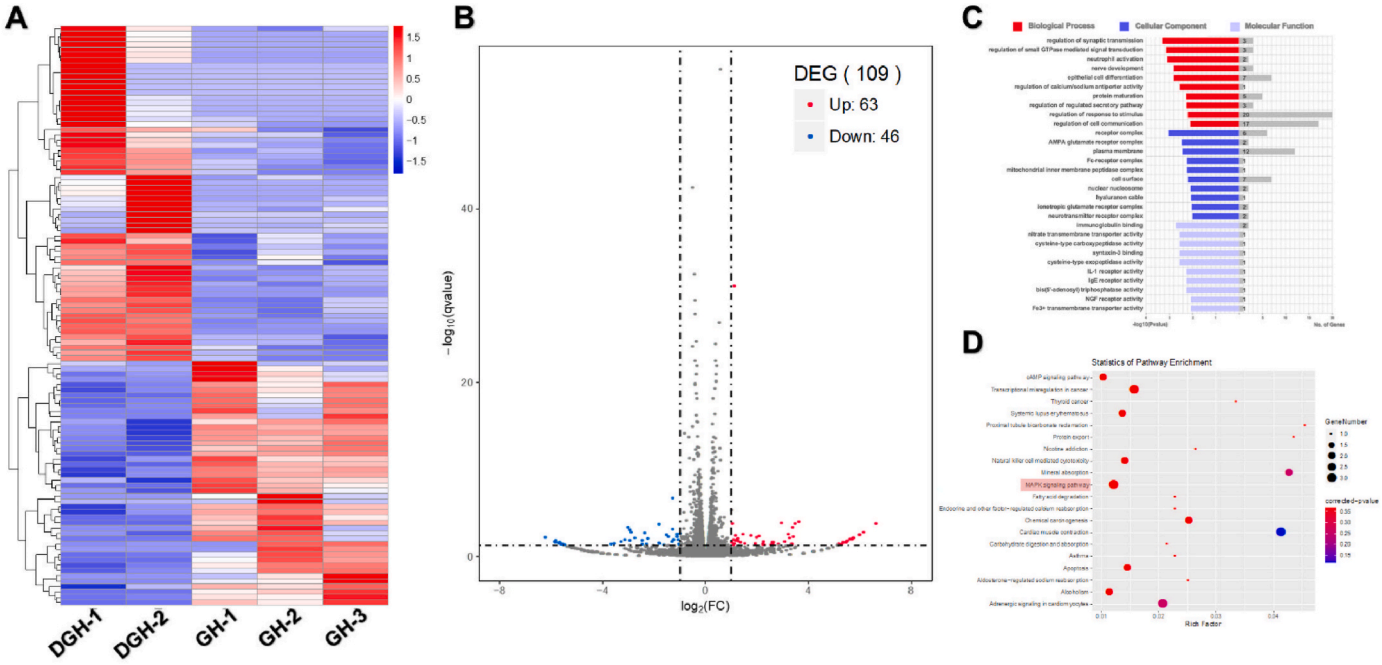

Fig. 5. RNA sequencing of hDPSCs encapsulated in DGH. (A) Hierarchical clustering analysis of differentially expressed genes (DEGs). (B) Volcano plot of DEGs. (C) GO analysis of DEGs, including details of biological process, cellular components and molecular functions. (D) KEGG pathway analysis of involved signaling pathways.

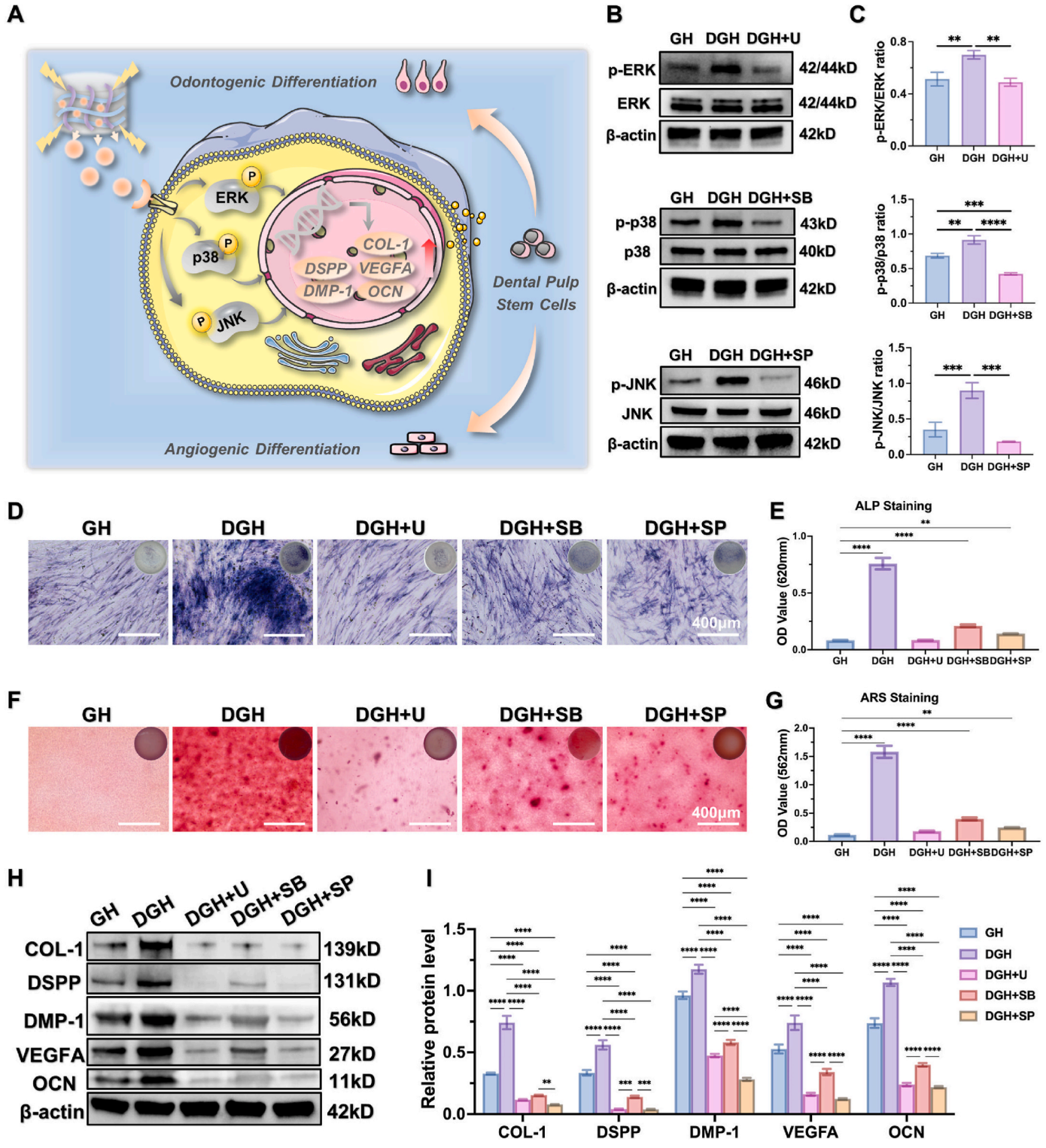

Fig. 6. Involvement of MAPK signals in DGH-mediated cell differentiation. (A) Schematic diagram of odontogenic and angiogenic promotion of DGH on hDPSCs via MAPK signals. (B) The expression of ERK, p38 and JNK MAPK in hDPSCs encapsulated in hydrogels in the absence or presence of pathway inhibitors. U0126 targeting ERK, SB203580 targeting p38 MAPK, and SP600125 targeting JNK. (C) Quantitative analysis of ERK, p38 and JNK MAPK proteins. (D) ALP staining of hDPSCs-encapsulated hydrogels in the absence or presence of pathway inhibitors. Scale bar: 400 μm. (E) Quantitative analysis of ALP activity. (F) ARS staining of hDPSCs-encapsulated hydrogels in the absence or presence of pathway inhibitors. Scale bar: 400 μm. (G) Quantitative analysis of mineralized nodules. (H) The expression of COL-1, DSPP, DMP-1, VEGFA and OCN proteins in hDPSCs encapsulated in hydrogels in the absence or presence of pathway inhibitors. (I) Quantitative analysis of COL-1, DSPP, DMP-1, VEGFA and OCN proteins. $^{****}p < 0.0001$, $^{***}p < 0.001$, $^{**}p < 0.01$, $^{*}p < 0.05$.

156.7 %, respectively, by comparison of the GH group, and could further be suppressed by corresponding inhibitors (Fig. 6B and C). In addition, the ALP activity and mineralized nodules deposition enhanced by DGH were dramatically descended to some extent in the presence of pathway inhibitors (Fig. 6D–G). The expression of COL-1, DSPP, DMP-1, VEGFA and OCN was also remarkably suppressed by inhibitors (Fig. 6H and I). Collectively, DGH contributed to a biomimetic microenvironment for cell differentiation through activation of pulp development-related intrinsic signals, among which ERK, p38 and JNK MAPK were pivotal players (Fig. 6A).

3.6. *In vivo regeneration of pulp/dentin-like tissue mediated by DGH*

To further mimic the microenvironment in mature permanent teeth, hDPSCs encapsulated in GH and DGH were injected into human root segments reserving narrow apical foramens and implanted into nude mice (Fig. 7A). The normal pulp group was used as a positive control (Fig. 7B). As shown in Fig. 7C–E, new tissue formation was visible in the cavities of each group. However, higher amounts of collagenous connective tissues were formed in the DGH group (Fig. 7F). Furthermore, in the interface of regenerated soft tissue and inner dentin of the DGH group was the linear arrangement cells concentrated on the border of the inner dentin wall, and their processes penetrated into the dentinal tubules, which was the most similar to the dentin-pulp complex (Fig. 7E). The newly formed tissues in the pure cells group showed no close integration with the inner dentin tubules and no structures similar to those of odontoblastic layers were observed (Fig. 7C). The predentin-like tissue could be found in the GH group, while it was irregular and relatively infrequent (Fig. 7D).

After transplantation, the surrounding cells of the hosts might also migrate through the apical foramina into the root canals. To determine whether the pulp tissue was regenerated by the implanted hDPSCs, immunofluorescence staining was performed using human mitochondrial antibodies, which only labeled the mitochondria of human cells but not the mitochondria in mouse cells. The results showed that most cells in the three groups expressed human mitochondria antigen (green), implying that the regenerated tissue cells were derived from implanted hDPSCs (Fig. 7G and I). Furthermore, DSPP and CD31 were co-stained in red to verify the regeneration of pulp-like tissues and the presence of blood vessels. In the pure cells group and the GH group, DSPP was expressed in small amounts in cells close to the dentin wall, while positive expression of DSPP that similar to the odontoblastic cells in native dental pulp tissues was observed in the DGH group (Fig. 7G). The number of positive cells in the three groups was counted and DSPP positive cells in the DGH group were significantly more ($p < 0.05$) (Fig. 7H). Moreover, some cells around blood vessels co-expressed human mitochondria and CD31, suggesting that some blood vessels were formed by the implanted hDPSCs (Fig. 7I). The number of blood vessels positively expressing human mitochondria was counted and it was found that the DGH group was the highest among the three groups (Fig. 7J). Our *in vivo* results proved that DGH provided a strong regenerative microenvironment and could promote the function of the transplanted cells.

4. Discussion

Recent development of stem cell-based regenerative medicine has broadened therapeutic horizons toward pulp regeneration with histological reconstruction and functional recovery [38,39]. However, the full-length pulp regeneration in mature permanent teeth is severely hindered by insufficient developmental signals and limited nutrient supply from narrow apical access. To address this, our study proposed a facile and efficient way to prepare DMEP, a cocktail of pulp tissue-specific proteins, and reconstructed the odontogenic microenvironment in root canals with the usage of a DMEP-functionalized hydrogel. Mechanistically, the hydrogel was found to mediate the pulp regeneration process by activating pulp developmental gene expressions and guiding the cell fate of hDPSCs. Our results revealed that the sufficient addition of extrinsic odontogenic induction signals was critical for supporting cell survival, proliferation, differentiation and safeguarding well-organized pulp-like tissues in root segments.

Dentin matrix was considered as a spontaneous reservoir of pulp-specific bioactive molecules and exhibited tremendous application potential in regenerative endodontic fields [15,16]. However, there is a striking difference in extracted components and therapeutic effects among various extraction procedures of dentin matrix proteins, and a standardized preparation protocol is absent [6]. The amounts of molecules released from dentin matrix depended on the ability of extracting agents to interfere with the protein-extracellular matrix interaction [40,41]. The influence of several demineralizing solutions and activation techniques, such as pH exposure, protease treatment, ultrasonication and heating, on growth factor release from dentin matrix has been previously evaluated [42]. Since the application of alkaline pulp capping agents could lead to localized demineralization, exposure of collagenous fibers and liberation of TGF-β1 from dentin matrix, we speculated that the release efficiency of dentin matrix proteins might be augmented under alkaline condition [43–45]. Thus, we investigated the pH value-/temperature-mediated release efficiency of DMEP and found that the maximum enrichment was achieved at pH 10/37 °C. Our study firstly proposed that a higher yield of DMEP could benefit from alkaline condition and elevated temperature treatment, and the extracting procedure was straightforward and reproducible. More importantly, the removal of collagen and mineral phase from DDM might reduce the immunogenicity of DMEP and then ameliorate host response and reach better regeneration effect, thus even xenogeneic DMEP harvested from different species such as swine, bovine, canine, goat and monkey might possess excellent histocompatibility and exhibit inspiring clinical application potential [46,47].

To deliver DMEP into root canals and achieve sustained release, an injectable double network hydrogel was fabricated. GelMA is a polyelectrolyte network structure with high crosslink density performing rigid and brittle, while HAMA is a neutral network structure with loose crosslink performing soft and tough, thus the mechanical strength and degradability of the double network hydrogel were superior to those of pure GelMA or HAMA, and could be customized through adjusting polymer concentrations according to tissues to be regenerated [30,48]. Our study indicated that the introduction of DMEP also improved the mechanical strength and decreased the degradation rate of the hydrogel. As the doping density of DMEP increased, the hydrogel met higher crosslinking degree and the biological behaviors of cells encapsulated in it changed. The rounded cell morphologies and restricted stretch in higher crosslinking networks were crucial for stemness maintenance. Hence, the enhancement of odontogenic and angiogenic differentiation of hDPSCs encapsulated in D_{10}GH may not only be ascribed to supplement of extrinsic odontogenic signals but also variation in mechanotransduction of the hydrogel, that is, the tunable and adjustable hydrogel could act as a stem cell ecological niche to support cell encapsulation, metabolism and differentiation [49].

Since the combinatorial application of multiple tissue-specific bioactive molecules and the double network hydrogel provided a biomimetic microenvironment for the encapsulation, proliferation, odontogenic and angiogenic differentiation of hDPSCs, the altered transcriptome and associated signaling pathways induced by DGH were further explored. The MAPK family, a group of serine/threonine protein kinases, weighs heavily for cytodifferentiation by transducing multiple extracellular signals to cellular responses and is composed of three main subfamilies: ERK, p38 and JNK MAPK [50]. According to previous reports, the ERK signaling pathway is involved in the regulation of cytodifferentiation, the p38 MAPK is responsible for regulating cytokine expression and could be activated by inflammatory cytokine signals, while the JNK MAPK is a stress-activated kinase associated with anti-proliferative and apoptotic functions [50,51]. Wu and colleagues

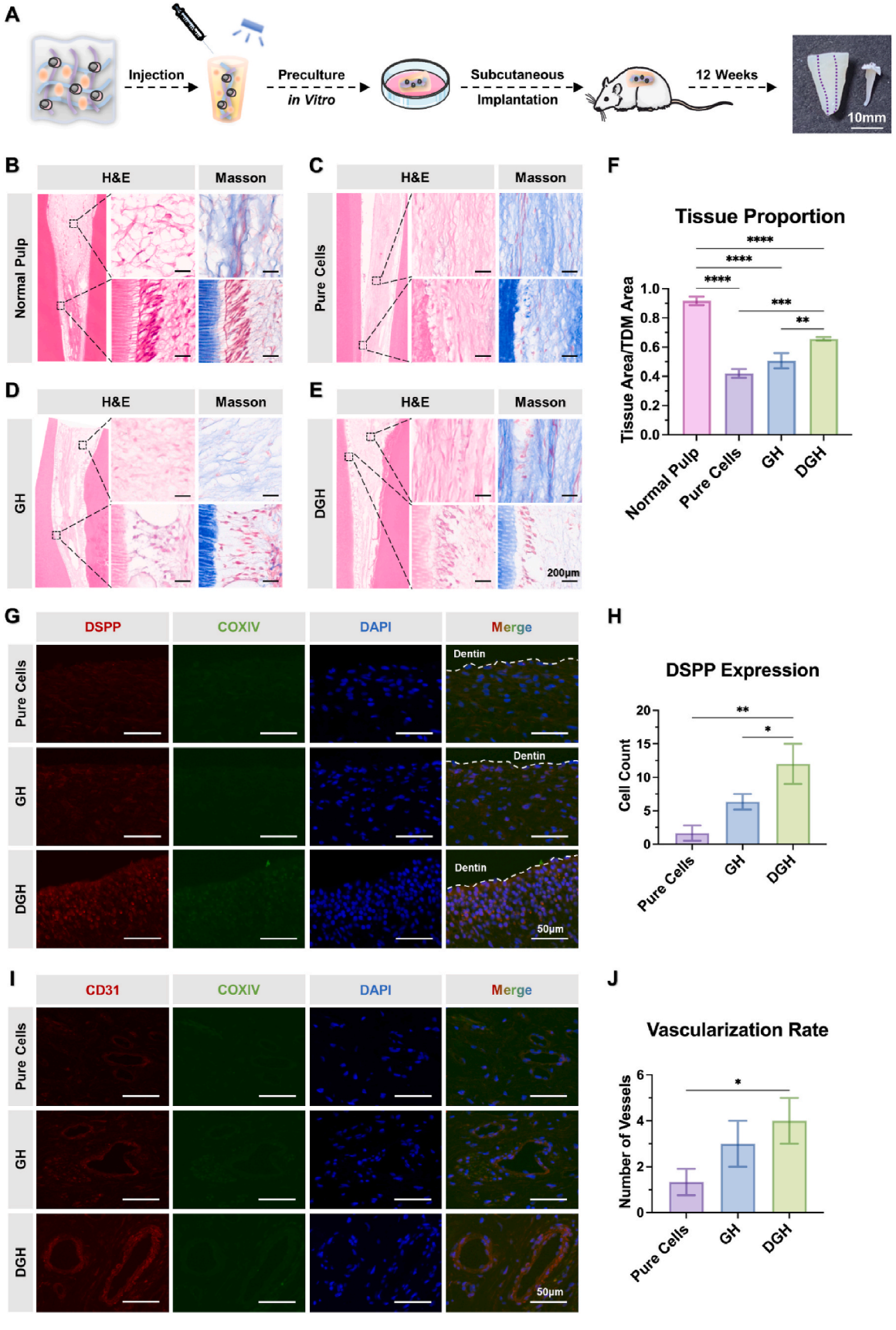

(caption on next page)

Fig. 7. Pulp-like tissue regeneration in hDPSCs/DGH-injected root segments after subcutaneous implantation into nude mice. (A) Schematic diagram of the *in vivo* implanting process. (B) H&E and Masson staining of normal pulp. (C–E) H&E and Masson staining of newly formed tissues in root segments injected with pure cells (C), cells-encapsulated GH (D), and cells-encapsulated DGH (E). Scale bar: 200 μm. (F) Quantitative analysis of the ratio of the pulp-like tissue area to the inner wall area of root segments (n = 5). (G) Immunofluorescence staining of DSPP and COXIV of newly formed tissues. DSPP positive cells were stained red, COXIV positive cells were stained green, and nuclei were stained blue. Scale bar: 50 μm. (H) Number of positive cells for DSPP (n = 5). (I) Immunofluorescence staining of CD31 and COXIV of newly formed tissues. CD31 positive cells were stained red, COXIV positive cells were stained green, and nuclei were stained blue. Scale bar: 50 μm. (J) Number of positive cells for CD31 (n = 5). ****$p < 0.0001$, ***$p < 0.001$, **$p < 0.01$, *$p < 0.05$. (For interpretation of the references to colour in this figure legend, the reader is referred to the Web version of this article.)

demonstrated that the conditioned medium of calcined tooth powder promoted the odontogenic differentiation of hDPSCs by inducing MAPK pathways [52]. In the present study, the phosphorylation of ERK, p38 and JNK MAPK was significantly increased in hDPSCs cultured with DGH, and blunting these signals with corresponding inhibitors blocked the effects of DGH on the odontogenic and angiogenic differentiation of hDPSCs. Interestingly, we observed that the inhibitory effect of U0126 and SP600125 was stronger than that of SB203580, indicating the ERK and JNK pathways may play a more important role in the DGH-induced differentiation of hDPSCs rather than p38. It should be noted that MAPK signaling pathways could interact with multiple signaling pathways such as BMP/Smad, Wnt/β-catenin, NF-κB and PI3K/AKT, thus further studies to figure out the detailed mechanisms were needed [51].

To mimic the clinical circumstance of mature permanent teeth, a semi-orthotopic pulp regeneration model was used in the study and a type of modified human root segments reserving narrow apical orifices was prepared. The segments were similar to natural roots in anatomical morphologies and material exchanges, which could provide a root canal-like environment to induce odontogenic and angiogenic differentiation of implanted hDPSCs. Our *in vivo* experiments revealed that more orderly and denser pulp-like tissues were regenerated in the DGH group, containing well-organized odontoblast-like mineralizing cells at sites in contact with dentin, as well as abundant collagenous fibers and blood vessels at the center of neotissues. The dentin and pulp form an inseparable unit because they are closely related functionally as well as embryologically and histologically, thus reassembling of odontoblasts is essential for successful pulp regeneration. Similar to our *in vivo* results, some previous studies also found that newly formed odontoblast-like cells were more likely to be observed on the inner surfaces of root segments although extrinsic inducing signals delivered by implanted biomaterials were distributed evenly in root canals [7,8,53]. These phenomena may be interpreted as the root segment provided a biological and morphological environment for the implanted complex during the regenerating process. On the one hand, residual active proteins embedded in root segments could induce the migration and odontogenic differentiation of stem cells; more importantly, root segments possess unique dentin tubule structures that tempt cytoplasmic projections of polarized odontoblast-like cells to extend into [8,54,55]. By contrast, newly formed tissues in the pure cells group and the GH group were disorganized and their odontoblast layers were unobservable, indicating that the regeneration events in root canals were coordinately regulated by intrinsic signals embedded in the inner dentin wall as well as extrinsic signals delivered by hydrogels, among which, the implanted hydrogel might play a more critical role due to osteogenic signals included in it were abundant and preactivated.

Neovascularization is a prerequisite for successful tissue regeneration; thus, some earlier studies have mixed human umbilical vein endothelial cells (HUVECs) with hDPSCs to promote vascular maturation [28,56]. Compared with hDPSCs, the source of HUVECs is more limited and the combined implantation of HUVECs and hDPSCs might increase the risk of immunological rejection. Our results indicated that DGH could mediate the regeneration of blood vessels depending on the elevated angiogenic differentiation of implanted hDPSCs, largely owing to angiogenesis-related factors embedded in DMEP. We speculated that the combinatorial application of developmentally pivotal signals of the dentin-pulp complex and the 3D biomimetic hydrogel recapitulated the developmental microenvironment for dental pulp and achieved inspiring regenerative effects.

Although an effective and reproducible bio-scaffold was fabricated in our study, there are still some drawbacks. First, DMEP we used was prepared from healthy premolar teeth of volunteers aged from 18 to 25, while the amounts of cytokines involved in DMEP extracted from different age groups should be further investigated to establish a standard preparation process and quality control. Second, *in situ* experiments on large animals with comparable "anatomical, physiologic, histologic, and pathologic characteristics to clinical situations" should be taken into account in future work.

5. Conclusion

This study reported a facile but efficient strategy to obtain pulp tissue-specific proteins (DMEP) and prepare a DMEP-functionalized biomimetic hydrogel (DGH). DGH well mimicked the ECM of native pulp, providing the most similar environment favorable for the adhesion, propagation, migration, odontogenic and angiogenic differentiation of hDPSCs. Besides, DGH as a cell delivery could induce the regeneration of highly organized and vascularized pulp-like tissues in root segments. Due to powerful fluidity and shape-adaptability, DGH was user-friendly to inject into complex root canal systems and could be crosslinked using UV light, exhibiting promising application and translation potential in future regenerative endodontic fields.

CRediT authorship contribution statement

Zhuo Xie: Writing – review & editing, Writing – original draft, Visualization, Methodology, Investigation, Conceptualization. **Peimeng Zhan:** Software, Investigation, Data curation. **Xinfang Zhang:** Software, Methodology, Data curation. **Shuheng Huang:** Formal analysis, Data curation. **Xuetao Shi:** Writing – review & editing, Funding acquisition. **Zhengmei Lin:** Writing – review & editing, Validation, Supervision, Resources, Project administration, Methodology, Funding acquisition. **Xianling Gao:** Writing – review & editing, Validation, Supervision, Resources, Project administration, Funding acquisition, Conceptualization.

Declaration of competing interest

The authors declare that they have no known competing financial interests or personal relationships that could have appeared to influence the work reported in this paper.

Data availability

Data will be made available on request.

Acknowledgments

This work was financially supported by the National Natural Science Foundation of China (No. 82001096, 82170939 and U22A20157) and the Natural Science Foundation of Guangdong Province (2022A1515010782 and 2021A1515010876).

References

[1] M. Zanini, E. Meyer, S. Simon, Pulp inflammation diagnosis from clinical to inflammatory mediators: a systematic review, J. Endod. 43 (7) (2017) 1033–1051.

[2] Y. Su, C. Wang, L. Ye, Healing rate and post-obturation pain of single- versus multiple-visit endodontic treatment for infected root canals: a systematic review, J. Endod. 37 (2) (2011) 125–132.

[3] Z. Siddiqui, A.M. Acevedo-Jake, A. Griffith, N. Kadincesme, K. Dabek, D. Hindi, K. K. Kim, Y. Kobayashi, E. Shimizu, V. Kumar, Cells and material-based strategies for regenerative endodontics, Bioact. Mater. 14 (2022) 234–249.

[4] L.M. Lin, G.T. Huang, A. Sigurdsson, B. Kahler, Clinical cell-based versus cell-free regenerative endodontics: clarification of concept and term, Int. Endod. J. 54 (6) (2021) 887–901.

[5] K. Xuan, B. Li, H. Guo, W. Sun, X. Kou, X. He, Y. Zhang, J. Sun, A. Liu, L. Liao, S. Liu, W. Liu, C. Hu, S. Shi, Y. Jin, Deciduous autologous tooth stem cells regenerate dental pulp after implantation into injured teeth, Sci. Transl. Med. 10 (455) (2018).

[6] X. Wei, M. Yang, L. Yue, D. Huang, X. Zhou, X. Wang, Q. Zhang, L. Qiu, Z. Huang, H. Wang, L. Meng, H. Li, W. Chen, X. Zou, J. Ling, Expert consensus on regenerative endodontic procedures, Int. J. Oral Sci. 14 (1) (2022) 55.

[7] H. Guo, B. Li, M. Wu, W. Zhao, X. He, B. Sui, Z. Dong, L. Wang, S. Shi, X. Huang, X. Liu, Z. Li, X. Guo, K. Xuan, Y. Jin, Odontogenesis-related developmental microenvironment facilitates deciduous dental pulp stem cell aggregates to revitalize an avulsed tooth, Biomaterials 279 (2021) 121223.

[8] X. Yuan, Z. Yuan, Y. Wang, Z. Wan, X. Wang, S. Yu, J. Han, J. Huang, C. Xiong, L. Ge, Q. Cai, Y. Zhao, Vascularized pulp regeneration via injecting simvastatin functionalized GelMA cryogel microspheres loaded with stem cells from human exfoliated deciduous teeth, Mater Today Bio 13 (2022) 100209.

[9] K. Xia, Z. Chen, J. Chen, H. Xu, Y. Xu, T. Yang, Q. Zhang, RGD- and VEGF-mimetic peptide epitope-functionalized self-assembling peptide hydrogels promote dentin-pulp complex regeneration, Int. J. Nanomed. 15 (2020) 6631–6647.

[10] C. Liang, L. Liao, W. Tian, Stem cell-based dental pulp regeneration: insights from signaling pathways, Stem Cell Rev Rep 17 (4) (2021) 1251–1263.

[11] A.W. James, G. LaChaud, J. Shen, G. Asatrian, V. Nguyen, X. Zhang, K. Ting, C. Soo, A review of the clinical side effects of bone morphogenetic protein-2, Tissue Eng., Part B 22 (4) (2016) 284–297.

[12] X. Han, L. Liao, T. Zhu, Y. Xu, F. Bi, L. Xie, H. Li, F. Huo, W. Tian, W. Guo, Xenogeneic native decellularized matrix carrying PPARγ activator RSG regulating macrophage polarization to promote ligament-to-bone regeneration, Mater. Sci. Eng., C 116 (2020) 111224.

[13] Y. Xu, J. Zhou, C. Liu, S. Zhang, F. Gao, W. Guo, X. Sun, C. Zhang, H. Li, Z. Rao, S. Qiu, Q. Zhu, X. Liu, X. Guo, Z. Shao, Y. Bai, X. Zhang, D. Quan, Understanding the role of tissue-specific decellularized spinal cord matrix hydrogel for neural stem/progenitor cell microenvironment reconstruction and spinal cord injury, Biomaterials 268 (2021) 120596.

[14] Z. Liang, J. Li, H. Lin, S. Zhang, F. Liu, Z. Rao, J. Chen, Y. Feng, K. Zhang, D. Quan, Z. Lin, Y. Bai, Q. Huang, Understanding the multi-functionality and tissue-specificity of decellularized dental pulp matrix hydrogels for endodontic regeneration, Acta Biomater. (2024) S1742-7061(24)00223-X.

[15] X. Gao, W. Qin, P. Wang, L. Wang, M.D. Weir, M.A. Reynolds, L. Zhao, Z. Lin, H.H. K. Xu, Nano-structured demineralized human dentin matrix to enhance bone and dental repair and regeneration, Appl. Sci. 9 (5) (2019) 1013.

[16] S. Liu, J. Sun, S. Yuan, Y. Yang, Y. Gong, Y. Wang, R. Guo, X. Zhang, Y. Liu, H. Mi, M. Wang, M. Liu, R. Li, Treated dentin matrix induces odontogenic differentiation of dental pulp stem cells via regulation of Wnt/β-catenin signaling, Bioact. Mater. 7 (2022) 85–97.

[17] Z. Xie, W. Jiang, H. Liu, L. Chen, C. Xuan, Z. Wang, X. Shi, Z. Lin, X. Gao, Antimicrobial peptide- and dentin matrix-functionalized hydrogel for vital pulp therapy via synergistic bacteriostasis, immunomodulation, and dentinogenesis, Adv. Healthcare Mater. (2024) e2303709.

[18] X. Gao, M. Guan, X. Liu, H.H.K. Xu, Q. Huang, L. Chen, S. Huang, Y. Xiao, X. Shi, Z. Lin, Sustained delivery of growth factors and alendronate using partially demineralized dentin matrix for endogenous periodontal regeneration, Appl. Mater. Today 22 (2021) 100922.

[19] D. Cunha, N. Souza, M. Moreira, N. Rodrigues, P. Silva, C. Franca, S. Horsophonphong, A. Sercia, R. Subbiah, A. Tahayeri, J. Ferracane, P. Yelick, V. Saboia, L. Bertassoni, 3D-printed microgels supplemented with dentin matrix molecules as a novel biomaterial for direct pulp capping, Clin. Oral Invest. 27 (3) (2023) 1215–1225.

[20] X. Gao, W. Qin, L. Chen, W. Fan, T. Ma, A. Schneider, M. Yang, O.N. Obianom, J. Chen, M.D. Weir, Y. Shu, L. Zhao, Z. Lin, H.H.K. Xu, Effects of targeted delivery of metformin and dental pulp stem cells on osteogenesis via demineralized dentin matrix under high glucose conditions, ACS Biomater. Sci. Eng. 6 (4) (2020) 2346–2356.

[21] Y. Chae, M. Yang, J. Kim, Release of TGF-β1 into root canals with various final irrigants in regenerative endodontics: an in vitro analysis, Int. Endod. J. 51 (12) (2018) 1389–1397.

[22] M. Widbiller, A. Eidt, S.R. Lindner, K.A. Hiller, H. Schweikl, W. Buchalla, K. M. Galler, Dentine matrix proteins: isolation and effects on human pulp cells, Int. Endod. J. 51 (Suppl 4) (2018) e278–e290.

[23] M. Widbiller, R.B. Driesen, A. Eidt, I. Lambrichts, K.A. Hiller, W. Buchalla, G. Schmalz, K.M. Galler, Cell homing for pulp tissue engineering with endogenous dentin matrix proteins, J. Endod. 44 (6) (2018) 956–962.e2.

[24] P. Noohi, M.J. Abdekhodaie, M.H. Nekoofar, K.M. Galler, P.M.H. Dummer, Advances in scaffolds used for pulp-dentine complex tissue engineering: a narrative review, Int. Endod. J. 55 (12) (2022) 1277–1316.

[25] L. Zheng, Y. Liu, L. Jiang, X. Wang, Y. Chen, L. Li, M. Song, H. Zhang, Y.S. Zhang, X. Zhang, Injectable decellularized dental pulp matrix-functionalized hydrogel microspheres for endodontic regeneration, Acta Biomater 156 (2023) 37–48.

[26] E. Ahmadian, A. Eftekhari, S.M. Dizaj, S. Sharifi, M. Mokhtarpour, A.N. Nasibova, R. Khalilov, M. Samiei, The effect of hyaluronic acid hydrogels on dental pulp stem cells behavior, Int. J. Biol. Macromol. 140 (2019) 245–254.

[27] N. Monteiro, G. Thrivikraman, A. Athirasala, A. Tahayeri, C.M. França, J. L. Ferracane, L.E. Bertassoni, Photopolymerization of cell-laden gelatin methacryloyl hydrogels using a dental curing light for regenerative dentistry, Dent. Mater. 34 (3) (2018) 389–399.

[28] A. Khayat, N. Monteiro, E.E. Smith, S. Pagni, W. Zhang, A. Khademhosseini, P. C. Yelick, GelMA-encapsulated hDPSCs and HUVECs for dental pulp regeneration, J. Dent. Res. 96 (2) (2017) 192–199.

[29] X. Liu, Y. Chen, A.S. Mao, C. Xuan, Z. Wang, H. Gao, G. An, Y. Zhu, X. Shi, C. Mao, Molecular recognition-directed site-specific release of stem cell differentiation inducers for enhanced joint repair, Biomaterials 232 (2020) 119644.

[30] W. Lu, M. Zeng, W. Liu, T. Ma, X. Fan, H. Li, Y. Wang, H. Wang, Y. Hu, J. Xie, Human urine-derived stem cell exosomes delivered via injectable GelMA templated hydrogel accelerate bone regeneration, Mater Today Bio 19 (2023) 100569.

[31] J. Guo, H. Yao, X. Li, L. Chang, Z. Wang, W. Zhu, Y. Su, L. Qin, J. Xu, Advanced Hydrogel systems for mandibular reconstruction, Bioact. Mater. 21 (2023) 175–193.

[32] P.S. Viana, M.O. Orlandi, A.C. Pavarina, A.L. Machado, C.E. Vergani, Chemical composition and morphology study of bovine enamel submitted to different sterilization methods, Clin. Oral Invest. 22 (2) (2018) 733–744.

[33] C. Gao, W.T. Sow, Y. Wang, Y. Wang, D. Yang, B.H. Lee, D. Matičić, L. Fang, H. Li, C. Zhang, Hydrogel composite scaffolds with an attenuated immunogenicity component for bone tissue engineering applications, J. Mater. Chem. B 9 (8) (2021) 2033–2041.

[34] Y. Zhang, J. Chen, H. Fu, S. Kuang, F. He, M. Zhang, Z. Shen, W. Qin, Z. Lin, S. Huang, Exosomes derived from 3D-cultured MSCs improve therapeutic effects in periodontitis and experimental colitis and restore the Th17 cell/Treg balance in inflamed periodontium, Int. J. Oral Sci. 13 (1) (2021) 43.

[35] H.S. Choi, J.W. Kim, Y.N. Cha, C. Kim, A quantitative nitroblue tetrazolium assay for determining intracellular superoxide anion production in phagocytic cells, J. Immunoassay Immunochem. 27 (1) (2006) 31–44.

[36] W. Qin, Z.M. Lin, R. Deng, D.D. Li, Z. Song, Y.G. Tian, R.F. Wang, J.Q. Ling, X. F. Zhu, p38a MAPK is involved in BMP-2-induced odontoblastic differentiation of human dental pulp cells, Int. Endod. J. 45 (3) (2012) 224–233.

[37] W. Qin, P. Liu, R. Zhang, S. Huang, X. Gao, Z. Song, R. Wang, L. Chen, B. Guo, Z. Lin, JNK MAPK is involved in BMP-2-induced odontoblastic differentiation of human dental pulp cells, Connect. Tissue Res. 55 (3) (2014) 217–224.

[38] B. Sui, C. Chen, X. Kou, B. Li, K. Xuan, S. Shi, Y. Jin, Pulp stem cell-mediated functional pulp regeneration, J. Dent. Res. 98 (1) (2019) 27–35.

[39] Z. Xie, Z. Shen, P. Zhan, J. Yang, Q. Huang, S. Huang, L. Chen, Z. Lin, Functional dental pulp regeneration: basic research and clinical translation, Int. J. Mol. Sci. 22 (16) (2021).

[40] S. Quijano-Guauque, L.J. Bernal-Cepeda, F.G. Delgado, J.E. Castellanos, C. García-Guerrero, Effect of chitosan irrigant solutions on the release of bioactive proteins from root dentin, Clin. Oral Invest. 27 (2) (2023) 691–703.

[41] K.M. Galler, W. Buchalla, K.A. Hiller, M. Federlin, A. Eidt, M. Schiefersteiner, G. Schmalz, Influence of root canal disinfectants on growth factor release from dentin, J. Endod. 41 (3) (2015) 363–368.

[42] D. Hancerliogullari, A. Erdemir, U. Kisa, The effect of different irrigation solutions and activation techniques on the expression of growth factors from dentine of extracted premolar teeth, Int. Endod. J. 54 (10) (2021) 1915–1924.

[43] L. Graham, P.R. Cooper, N. Cassidy, J.E. Nor, A.J. Sloan, A.J. Smith, The effect of calcium hydroxide on solubilisation of bio-active dentine matrix components, Biomaterials 27 (14) (2006) 2865–2873.

[44] P.L. Tomson, P.J. Lumley, A.J. Smith, P.R. Cooper, Growth factor release from dentine matrix by pulp-capping agents promotes pulp tissue repair-associated events, Int. Endod. J. 50 (3) (2017) 281–292.

[45] S. Wang, Y. Niu, P. Jia, Z. Liao, W. Guo, R.C. Chaves, K.H. Tran-Ba, L. He, H. Bai, S. Sia, L.J. Kaufman, X. Wang, Y. Zhou, Y. Dong, J.J. Mao, Alkaline activation of endogenous latent TGFβ1 by an injectable hydrogel directs cell homing for in situ complex tissue regeneration, Bioact. Mater. 15 (2022) 316–329.

[46] F. Bi, Z. Zhang, W. Guo, Treated dentin matrix in tissue regeneration: recent advances, Pharmaceutics 15 (1) (2022).

[47] T. Wang, Y. Guo, The host response to autogenous, allogeneic, and xenogeneic treated dentin matrix/demineralized dentin matrix-oriented tissue regeneration, Tissue Eng., Part B 30 (1) (2024) 74–81.

[48] P. Xu, L. Lou, W. Zhan, C. Wang, S. Wu, Z. Liu, Y. Wang, Bicomponent hydrogel laden with TGF-β3-nucleus pulposus stem cells for disc degeneration repair, Chem. Eng. J. 479 (2024) 147788.

[49] O. Chaudhuri, J. Cooper-White, P.A. Janmey, D.J. Mooney, V.B. Shenoy, Effects of extracellular matrix viscoelasticity on cellular behaviour, Nature 584 (7822) (2020) 535–546.

[50] G.L. Johnson, R. Lapadat, Mitogen-activated protein kinase pathways mediated by ERK, JNK, and p38 protein kinases, Science 298 (5600) (2002) 1911–1912.

[51] L. Zhou, S. Zhao, X. Xing, Effects of different signaling pathways on odontogenic differentiation of dental pulp stem cells: a review, Front. Physiol. 14 (2023) 1272764.

[52] J. Wu, N. Li, Y. Fan, Y. Wang, Y. Gu, Z. Li, Y. Pan, G. Romila, Z. Zhou, J. Yu, The conditioned medium of calcined tooth powder promotes the osteogenic and odontogenic differentiation of human dental pulp stem cells via MAPK signaling pathways, Stem Cell. Int. 2019 (2019) 4793518.

[53] N. Luo, Y.W. Deng, J. Wen, X.C. Xu, R.X. Jiang, J.Y. Zhan, Y. Zhang, B.Q. Lu, F. Chen, X. Chen, Wnt3a-Loaded hydroxyapatite Nanowire@Mesoporous silica core-shell nanocomposite promotes the regeneration of dentin-pulp complex via angiogenesis, oxidative stress resistance, and odontogenic induction of stem cells, Adv. Healthcare Mater. 12 (22) (2023) e2300229.
[54] S.N. Kaushik, B. Kim, A.M. Walma, S.C. Choi, H. Wu, J.J. Mao, H.W. Jun, K. Cheon, Biomimetic microenvironments for regenerative endodontics, Biomater. Res. 20 (2016) 14.
[55] K.M. Galler, R.N. D'Souza, M. Federlin, A.C. Cavender, J.D. Hartgerink, S. Hecker, G. Schmalz, Dentin conditioning codetermines cell fate in regenerative endodontics, J. Endod. 37 (11) (2011) 1536–1541.
[56] Q. Liang, C. Liang, X. Liu, X. Xing, S. Ma, H. Huang, C. Liang, L. Liu, L. Liao, W. Tian, Vascularized dental pulp regeneration using cell-laden microfiber aggregates, J. Mater. Chem. B 10 (48) (2022) 10097–10111.